Supersonic Aeroelastic Applications of Harmonic Potential Panel Method to Oscillating Flexible Bodies

Pablo Garcia-Fogeda* and D. D. Liu†
Arizona State University, Tempe, Arizona

For supersonic aeroelastic applications, the Harmonic Potential Panel (HPP) method for elastic bodies in oscillatory motion is presented. For applicability in the full supersonic-flow regime, the HPP method has been extended to include the mean-flow nonlinearity according to Van Dyke's nonlinear iterative scheme. In all computed cases, improvements are found for the HPP nonlinear results over the HPP linear results. Effects of frequency upon generalized forces for two different body shapes are investigated. Rigid body oscillation flutter boundaries and free-free body bending aerodynamic damping coefficients are presented for various configurations, including Hanson and Doggett's SA-1 launch vehicle model. Overall trends are established and favorable comparisons obtained with measured data throughout the supersonic Mach number range.

Nomenclature

C_p = total pressure coefficient
C_{p1} = unsteady pressure coefficient
C_{p0} = mean-flow pressure coefficient
e_x, e_r, e_θ = body-fixed unit vectors
$g(x)$ = normalized natural mode shape
M_∞ = freestream Mach number
t = time in a coordinate system moving relative to freestream
x, r, θ = cylindrical coordinates
β = $\sqrt{M^2 - {}_\infty 1}$
δ_0 = amplitude of oscillation
ξ = dipole coordinate
τ = time in a wind-fixed system
τ_0 = body thickness ratio
ϕ_0 = mean-flow perturbation potential
ϕ_1 = unsteady flow perturbation potential

I. Introduction

RENEWED interest in the slender-body aeroelasticity is due to current designs of a new class of missiles and launch vehicles. In particular, these bodies with long, slender configurations are susceptible to a number of aeroelastic instabilities during supersonic flights. For body-fin configurations, flutter is likely to occur when the short-period rigid body-fin mode and the body bending mode are properly phased.

To assess these aeroelastic instabilities one requires primarily an accurate prediction method in computing the unsteady aerodynamics. To date, no work appears available in treatments of oscillating flexible bodies at high speeds. Our objective is, therefore, to address this problem area and to present the newly developed Harmonic Potential Panel (HPP) method[1] and its computed instability boundaries in the supersonic regime.

Unlike the formulation for wings,[2] the unsteady airloads are influenced by the mean-flow through the boundary condition and the unsteady pressures in the HPP formulation. Hence, in addition to the developed HPP method, a nonlinear mean-flow model is formulated and incorporated into the HPP code for flutter computations. The HPP method adopts the body-fixed coordinate system and a line-doublet paneling scheme (see Fig. 1). It is completely general for any given pointed body, and its oscillation frequency is valid in the full range. Conventional panel methods require panels around the body surface in several hundreds.[3] By contrast, the present method typically requires one-tenth of this amount. Furthermore, the panel number is not significantly affected by the Mach number and frequency variations.

To validate the HPP method, the computed results in various limits are verified with various known supersonic theories. Favorable comparisons with measured data are obtained for all instability boundaries, including that of Hanson and Doggett's Saturn SA-1 launch vehicle model.

II. Analysis

As shown in Fig. 1a, the body-fixed coordinate system chosen requires that the x axis remain the axis of the body at all times, whereby each right cross section is circular and contains the r axis. Let Ω be the full velocity potential; the perturbed solutions of small amplitude $\delta(\tau)$ are sought in the following form:

$$\Omega(x,r,\theta,\tau) = x + g'(x)\delta(\tau)r\cos\theta + \phi_0(x,r) + \delta(\tau)\phi_1(x,r)\cos\theta \tag{1}$$

The total velocity in this curvilinear coordinate system is obtained

$$\nabla\Omega = [1 + \phi_{0x} - \delta(\tau)g''\phi_{0x}r\cos\theta + \delta(\tau)\phi_{1x}\cos\theta]e_x + [\phi_{0r} + \delta(\tau)\phi_{1r}\cos\theta + g'\delta(\tau)\cos\theta]e_r - \delta(\tau)[g'\sin\theta + (1/r)\phi_1\sin\theta]e_\theta \tag{2}$$

where ∇ represents the gradient operator.

The partial derivative with respect to τ as measured by an observer moving with the harmonically oscillating body-axis system (x, r, θ, t) is given by

$$\frac{\partial}{\partial\tau} = \frac{\partial}{\partial t} - g'\dot{\delta}(t)r\cos\theta\frac{\partial}{\partial x} + g\dot{\delta}(t)\left(\cos\theta\frac{\partial}{\partial r} - \frac{1}{r}\sin\theta\frac{\partial}{\partial\theta}\right) \tag{3}$$

Note that Eqs. (1-3) contain Revell's equations[4] for rigid-body oscillations as a special case.

Presented as Paper 86-0864 at the AIAA/ASME/ASCE/AHS 27th Structures, Structural Dynamics and Materials Conference, San Antonio, TX, May 19-21, 1986; received April 6, 1987; revision received Jan. 2, 1988.

*Faculty Associate, Mechanical and Aerospace Engineering. Member AIAA.

†Associate Professor, Mechanical and Aerospace Engineering. Member AIAA.

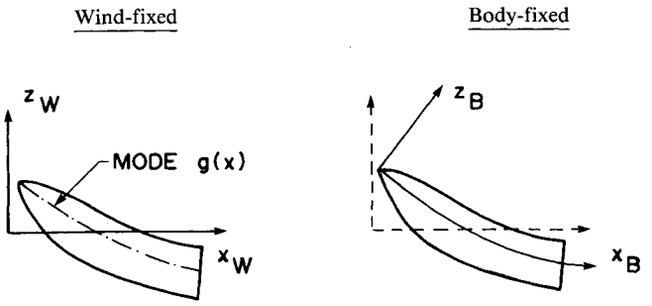

Fig. 1a Wind-fixed and body-fixed coordinate systems.

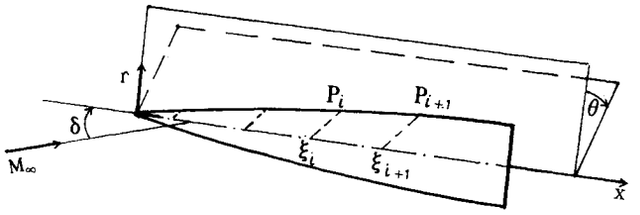

Fig. 1b Panel arrangement for axisymmetric bodies.

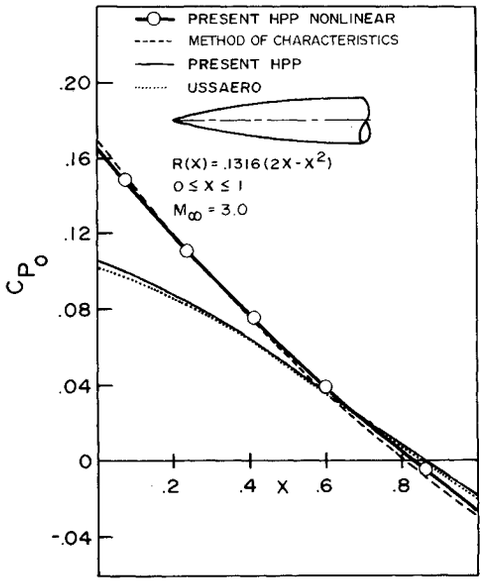

Fig. 2 Mean-flow pressures for a parabolic ogive at $M_\infty = 3.0$ and angle of attack $\alpha_0 = 0$ deg.

The governing equations for the mean-flow potential and unsteady-flow potential are, respectively,

$$-\beta^2\phi_{0xx} + \phi_{0rr} + (1/r)\phi_{0r} = M_\infty^2[(\gamma-1)(\phi_{0xx} + \phi_{0rr} + \phi_{0r}/r)/2 \times (2\phi_{0x} + \phi_{0x}^2 + \phi_{0r}^2) + 2\phi_{0xr}(1+\phi_{0x})\phi_{0r} + \phi_{0xx}(2\phi_{0x} + \phi_{0x}^2) + \phi_{0r}\phi_{0rr}] \quad (4)$$

$$-\beta^2\phi_{1xx} + \phi_{1rr} + (1/r)\phi_{1r} - (1/r^2)\phi_1 - 2ik\,M_\infty^2\phi_{1x} + M_\infty^2 k^2\phi_1 = G(g,\phi_0) \quad (5)$$

where G is the inhomogeneous term that can be found in Ref. 1; γ is the specific heat ratio of the gas; and k is the reduced frequency defined by $k = \omega L/U_\infty$, L is the characteristic body length and ω is the circular frequency.

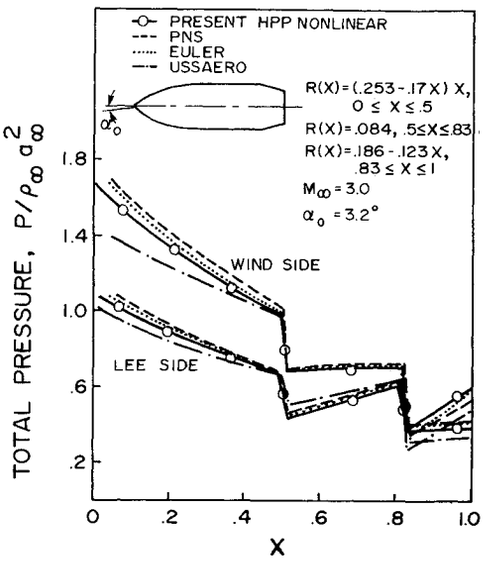

Fig. 3 Total pressure distributions of an ogive-cylinder boat-tail body at $M_\infty = 3.0$ and angle of attack $\alpha_0 = 3.2$ deg.

Mean-Flow Solutions

According to Van Dyke,[5] Eq. (4) can be solved by an iterative procedure. Letting $L(\cdot)$ be the left-hand-side operator and $R(\cdot)$ the right-hand-side operator, Eq. (4) can be simply expressed as $L(\phi_0) = R(\bar{\phi}_0)$. The potential $\bar{\phi}_0$ is the initial solution obtained by solving the linearized equation $L(\bar{\phi}_0) = 0$. To solve for the first iteration solution ϕ_0, we make use of Van Dyke's particular solution

$$\psi_0 = M_\infty^2[\bar{\phi}_{0x}(\bar{\phi}_0 + Nr\bar{\phi}_{0r}) - (r/4)\bar{\phi}_{0r}^3]$$

where

$$N = (\gamma+1)M_\infty^2/[2(M_\infty^2 - 1)] \quad (6)$$

This particular solution accounts for all second-order terms in $R(\bar{\phi}_0)$. Hence, ϕ_0 can be expressed as

$$\phi_0 = \chi_0 + \psi_0 \quad (7)$$

where χ_0 satisfies $L(\chi_0) = 0$. In terms of paneling scheme, χ_0 is determined by satisfying the tangency condition, i.e.,

$$\left\{\left[\left(\frac{\partial\chi_0}{\partial r}\right)_{ji}\right] - R'(x_j)\left[\left(\frac{\partial\chi_0}{\partial x}\right)_{ji}\right]\right\}\{C_i\} = [R'(x_j)] - \left\{\frac{\partial\psi_0}{\partial r}\left[x_j, R(x_j)\right]\right\} + \left\{R'(x_j)\frac{\partial\psi_0}{\partial x}\left[x_j, R(x_j)\right]\right\} \quad (8)$$

where j and i denote the locations of the control point and the sending point, respectively. In the subsequent development, both the linear solution $\bar{\phi}_0$ and the iterative nonlinear solution ϕ_0 are used to compute the stability and flutter boundaries, as shown in Figs. 4, 7, and 8.

Harmonic Dipole Potential

Following the basic formulation of Garcia-Fogeda and Liu,[1] there is obtained the integral solution of Eq. (5):

$$\phi_1(x,r) = -\frac{1}{2\pi}\int_x^{\beta r}\frac{\partial}{\partial x_0}[F(x-x_0)e^{-i\mu x_0}] \times S(x_0,\beta r)\,dx_0 + I[G] \quad (9)$$

where

$$S(x_0,\beta r) = \frac{\partial}{\partial r}\int_{\beta r}^{x_0} \frac{\cos(\lambda R_\sigma)}{R_\sigma}\,d\sigma$$

$$x_0 = x - \xi, \quad R_\sigma = \sqrt{\sigma^2 - \beta^2 r^2}, \quad \lambda = \frac{kM_\infty}{\beta^2}, \quad \text{and} \quad \mu = \frac{kM_\infty}{\beta^2}$$

$F(x - x_0)$ is the strength of the dipole distribution along the body axis, and $I[G]$ represents the inhomogeneous solution that is set to zero here since we are seeking the solution of the first-order equation for the crossflow.

Equation (9) is solved by discretizing the line-doublet elements along the body axis (i.e., ξ_i to ξ_{i+1}), whereas the potential ϕ_1 is evaluated at the discrete field points (x_j, r_j) along the Mach wave emanating from ξ_{j+1} (see Fig. 1b), i.e.,

$$\phi_1(x_j,r_j) = -\frac{1}{2\pi}\sum_{i=1}^{j}\int_{x_j-\xi_i}^{x_j-\xi_{i+1}} \frac{\partial}{\partial x_0}[F_i(x_j - x_0)e^{-i\mu x_0}] \times S(x_0,\beta r_j)\,dx_0 \tag{10}$$

The Harmonic-Gradient concept of Chen and Liu[2] is adopted to model the integrand of Eq. (10), i.e.,

$$\frac{\partial}{\partial x_0}[F_i(x_j - x_0)e^{-i\mu x_0}] = [a_i(x_j - x_0) + b_i]e^{-i\mu x_0} \tag{11}$$

where a_i and b_i are complex constants, and the right-hand side represents a linear-harmonic doublet gradient.

By applying the condition of the dipole strength continuously between adjacent elements, b_i can be related to a_i. The tangency condition, in terms of matrix notation, then reads

$$([V_{ji}] - R'(x_j)\,[U_{ji}])\,\{a_i\} = \{B_j\} \tag{12}$$

where $\{B_j\}$ is a column vector that depends on the given mode shape $g(x)$ and the mean-flow solution $\phi_0(x, r)$, evaluated at the control point x_j, $R(x_j)$, and $[U_{ji}]$, and $[V_{ji}]$ are lower tridiagonal matrices for the velocity influence coefficients of the oscillatory flow.

Generalized Forces

The exact isentropic pressure coefficient is expanded to yield the mean flow and the unsteady-flow pressure coefficients

$$C_p = C_{p0} + C_{p1}\delta_0 e^{ikt}\cos\theta \tag{13}$$

where C_{p1} only represents the first harmonic component of the total unsteady pressure, which can be expressed in terms of an in-phase (real) and an out-of-phase (imaginary) part. Thus, the generalized forces for a flexible body can be written

$$Q_{IJ} = -\frac{1}{S_{\text{ref}}}\int_0^{2\pi}\int_0^1 C_{p1}^{(J)} R(x) \times \left[g^{(I)} + RR'\frac{dg^{(I)}}{dx}\right]\cos^2\theta\,d\theta\,dx \tag{14}$$

where $g^{(I)}$ is the Ith structure mode, $C_{p1}^{(J)}$ is the pressure due to the Jth mode, and S_{ref} is the reference area of the body, usually being the base area.

Let "1" denote the plunging mode and "2" the pitching mode. The damping-in-pitch force and moment coefficients can then be determined, respectively, from the generalized forces in the following forms:

$$C_{N_\alpha} + C_{N_q} = -Im(Q_{12})/k \tag{15a}$$

$$C_{M_\alpha} + C_{M_q} = -Im(Q_{22})/k \tag{15b}$$

III. Results and Discussion

Nonlinear Results

Mean-flow pressures for a parabolic ogive are computed based on the linear and nonlinear iterative methods according to Eqs. (4-7). Figure 2 shows that the results of the present HPP linear method and nonlinear method are in excellent agreement with those obtained by USSAERO Code[6] (linear) and by the method of characteristics.[7] Large discrepancy is found between the linear and the nonlinear results. Next in Fig. 3, the nonlinear iterative method is applied to an ogive-cylinder boat-tail body at Mach number $M_\infty = 3.0$ and at angle of attack $\alpha_0 = 3.2$ deg. The present nonlinear results are in good agreement with those of the parabolized Navier-Stokes (PNS) code and the Euler code.[8] Considerable deviation between the linear and the nonlinear results can be seen at the apex of the windward side.

In the figures that follow, the legend "Present HPP" represents the HPP linear results to distinguish them from the "Present HPP nonlinear" results.

In Fig. 4, good agreement of HPP nonlinear results with Brong's Euler unsteady result[9] is obtained for the pitch-damping forces for a cone. The linear result is seen to deviate from the nonlinear ones as the Mach number increases. The nonlinear effect is enhanced by either increasing the hypersonic parameter $M_\infty\tau_0$ or decreasing the Mach number toward the transonic range. Hence, the HPP method is improved by the nonlinear scheme to handle problems in the low- or high-supersonic regime, provided that the effect of rotationality is negligible. These improved results prompt further pursuit of the nonlinear method for aeroelastic applications. As expected, improved trends of the flutter boundaries are obtained when the nonlinearity in the mean flow is included, as shown in Figs. 7 and 8. It is seen that the unsteady aerodynamics can be altered substantially by the mean-flow influence through the tangency condition and the pressure coefficient. Using computational fluid dynamics (CFD) means to obtain mean-flow solutions, such as using the Euler code or the PNS code, is generally expensive. As may be seen in Figs. 2 and 3, the present nonlinear results achieve the same accuracy but maintain low cost in computation. In this way, the HPP nonlinear method becomes compatible as an efficient tool for aeroelastic applications.

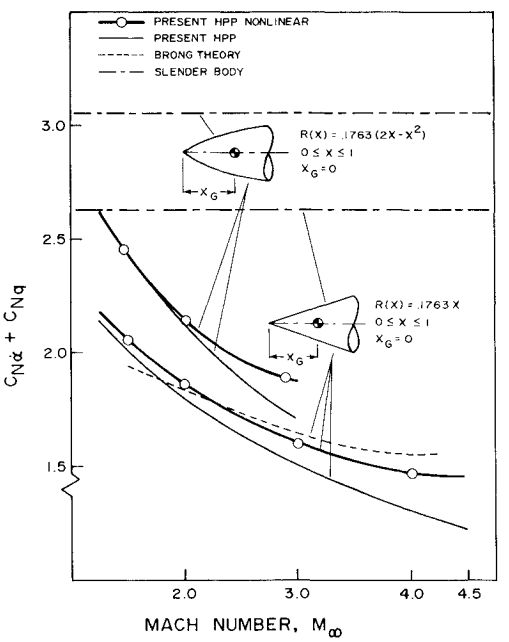

Fig. 4 Damping-in-pitch normal force coefficients vs Mach number for a cone and a parabolic ogive.

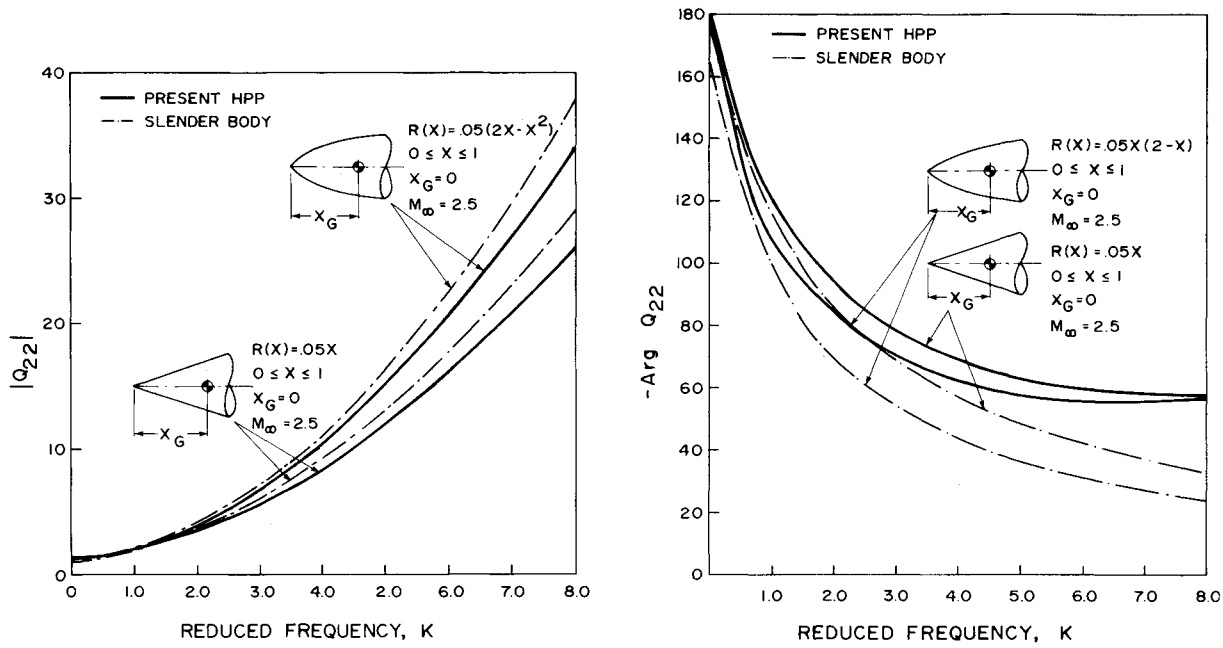

Fig. 5 Modulus and argument of the generalized forces vs reduced frequency for a cone and parabolic ogive in pitching mode at $M_\infty = 2.5$.

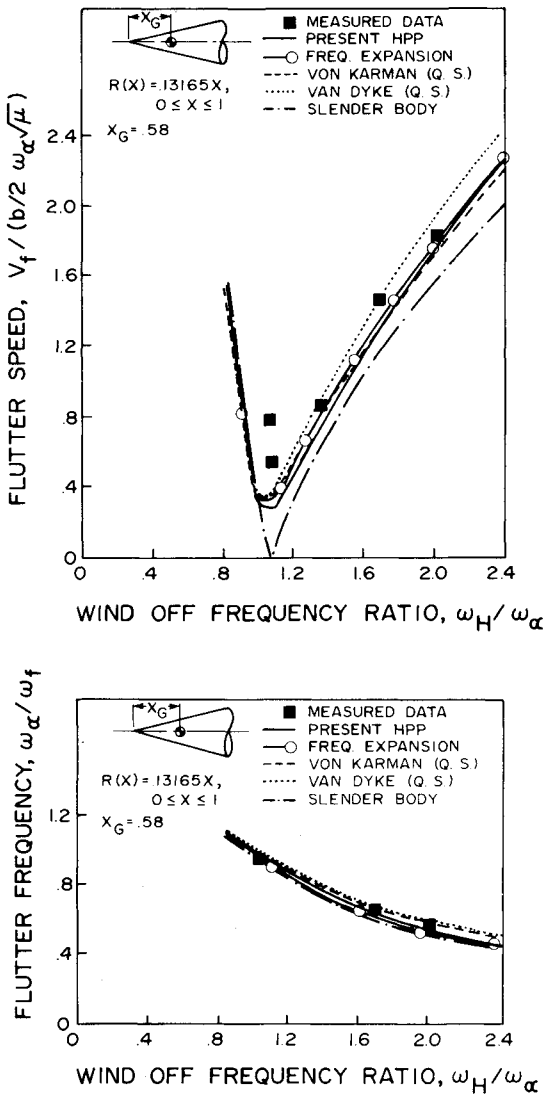

Fig. 6 Flutter boundaries for a 7.5 deg cone at $M_\infty = 2.0$ (data taken from Ref. 13).

Effects of Frequency

As shown in Ref. 1, the HPP method in the low-frequency limit and in the high-frequency limit has been verified with the linearized characteristic method[10] and the piston theory,[11] respectively. Across the frequency range, the modulus and the phase angle of the generalized forces Q_{22} for a cone and an ogive in pitching oscillations are presented in Fig. 5. It should be noted that the effects of body shape become apparent in the high-frequency range. All results merge in the low-frequency limit, as expected. Similar trends are found in the sonic-flow studies by Landahl.[12]

Flutter Boundaries

In Fig. 6, the flutter boundaries for a 7.5 deg cone at $M_\infty = 2.0$ in pitching and plunging modes are presented. It is seen that the slender-body theory results in the most conservative flutter boundary. While various quasisteady methods fail to predict the measured flutter speed,[13] the present HPP method only slightly underpredicts the flutter speed throughout the windoff frequency range.

In Figs. 7 and 8, the present HPP (linear) and its nonlinear methods are used to compute flutter boundaries for the same cone at a windoff frequency ratio $\omega_h/\omega_\alpha = 1.8$ for various Mach numbers. It is seen that consistent improvement in trends is obtained for the nonlinear results over the linear ones when compared with measured data.[13] However, the predicted boundaries become less conservative in the order of slender body, the HPP-linear and the HPP-nonlinear results. For the flutter boundaries presented in Figs. 7 and 8, overall trends in the predicted flutter speeds and frequencies are comparable to those measured. Since the cone is slender (cone semi-angle = 7.5 deg), the predicted flutter speeds by the linear and nonlinear methods merge in the low Mach number range. Similar trends can be observed in the mean-flow pressure distributions.[5] It should be noted that when the body becomes thicker, the linear and nonlinear results are expected to deviate from each other, as confirmed by Van Dyke for the mean flow.

Elastic Bodies

In Figs. 9 and 10, the in-phase and the out-of-phase pressures for two bodies oscillating in the free-free first and second bending modes are presented. These bodies include a parabolic ogive and a cone-cylinder of 10% thickness. At a given set of

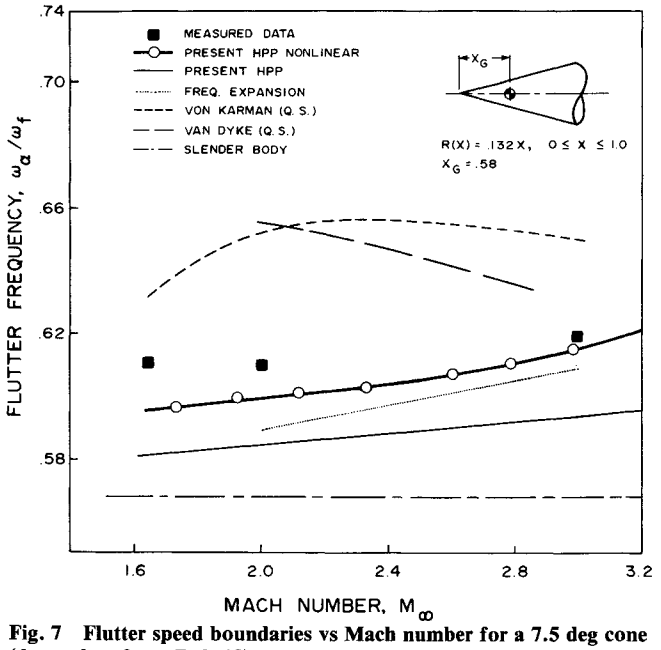

Fig. 7 Flutter speed boundaries vs Mach number for a 7.5 deg cone (data taken from Ref. 13).

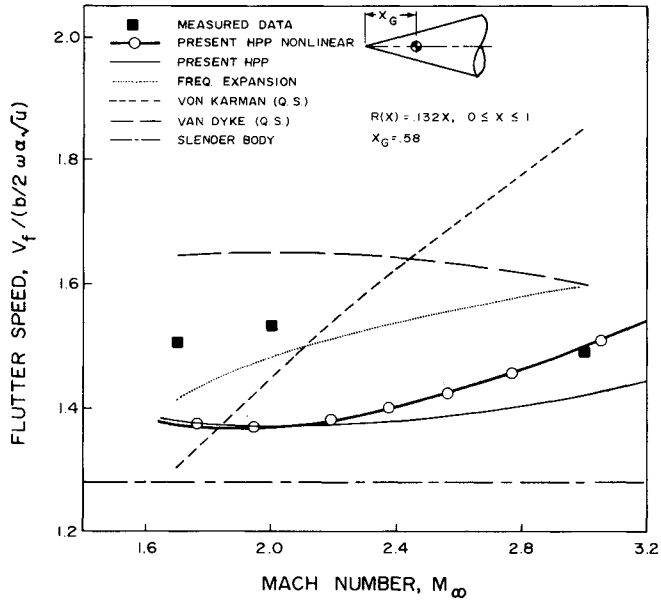

Fig. 8 Flutter frequency boundaries vs Mach number for a 7.5 deg cone (data taken from Ref. 13).

Mach number and reduced frequency ($M_\infty = 2.5$ and $k = 1.0$), it is observed that the second mode of oscillation results in larger magnitude in the in-phase pressure, and that the out-of-phase pressures resemble the mode shapes. The reason for this can be simply analyzed from the slender-body limit. That is, the out-of-phase pressure is proportional to the derivative of $R(x) \cdot g(x)$ and $R(x)$ vanishes at the apex, thus $R'(x)g(x)$ becomes the dominant term. For the cone-cylinder, the pressure jumps obviously result from the expansion waves generated at the shoulder.

Next, the computed results of the HPP method for an elastic cone-cylinder body oscillating in second bending mode are compared with the aerodynamic damping data measured by Hanson and Doggett.[14] The aerodynamic damping derivative is defined by

$$C_h = 2k\mu\left(\frac{C_A}{C_{cr}}\right) = -\frac{Im(Q_{II})}{\pi k}$$

where μ is the mass ratio. Physically, it represents the ratio of aerodynamic damping to the critical damping. The reduced frequency of the second bending mode lies between 2.9 and 4.2 corresponding to the Mach-number range of $M_\infty = 3.0$ to 1.5 (Fig. 11). It is seen that present results establish close trends with the measured data. By contrast, all quasisteady theories yield inferior predictions. Because of an inconsistent formulation, Bond and Packard's theory[15] results in considerable discrepancy, as may be seen in Fig. 11.

Saturn Launch Vehicle Model

Aeroelastic analyses of Hanson and Doggett's SA-1 launch vehicle model are presented in Figs. 12 and 13. This model was used by Hanson and Doggett to obtain aeroelastic measured data for the Saturn SA-1 launch vehicle.[16] Steady mean-flow pressure, in-phase and out-of-phase pressures are computed for the modeled vehicle in rigid mode in Fig. 12. The in-phase and out-of-phase pressures practically follow the same trend as that predicted by the slender-body theory. Clearly, the deviation between the slender-body results and the present HPP results are due to the Mach number and the thickness effects.

The measured mode shape[16] is used as the input for computing the aerodynamic damping coefficients. The aerodynamic damping coefficient is redefined here as $C_h = -Im(Q_{33})/(\pi k \eta)$, where "3" denotes the first bending mode and η is a parameter involving the body shape and the mode shape ($\eta = 1.763$—see Ref. 16). The natural frequency for the actual vehicle is 2.8 Hz; however, for the wind-tunnel model it is 153 Hz. Correspondingly, the reduced frequency lies between 1.4 to 2.53 for Mach range between 3.0 to 1.2, respectively. It should be noted that because of the substantial reduction in the model size, the reduced frequency is of order unity. Hence, the present case of study mandates a general solution, which can

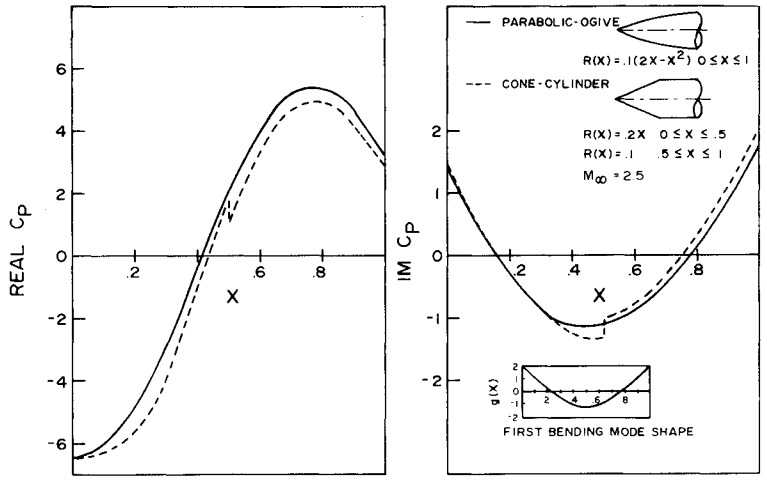

Fig. 9 In-phase and out-of-phase pressure coefficients for a cone-cylinder and a parabolic ogive in first-bending mode at $M_\infty = 2.5$ and reduced frequency $k = 1.0$.

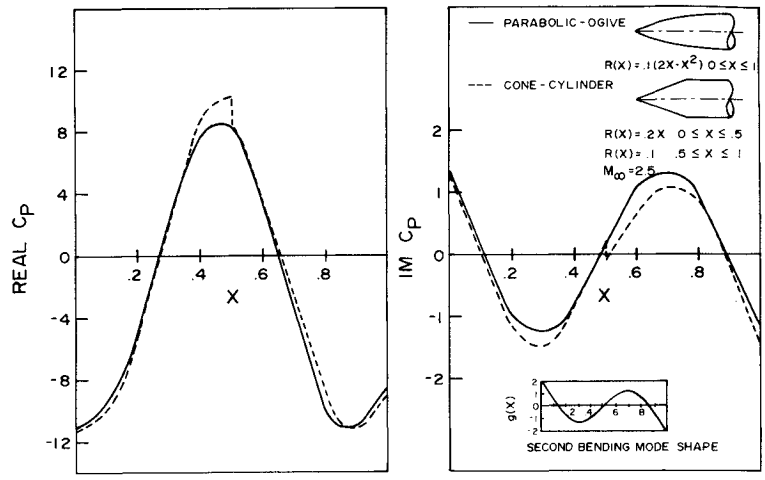

Fig. 10 In-phase and out-of-phase pressure coefficients for a cone-cylinder and a parabolic ogive in second-bending mode at $M_\infty = 2.5$ and reduced frequency $k = 1.0$.

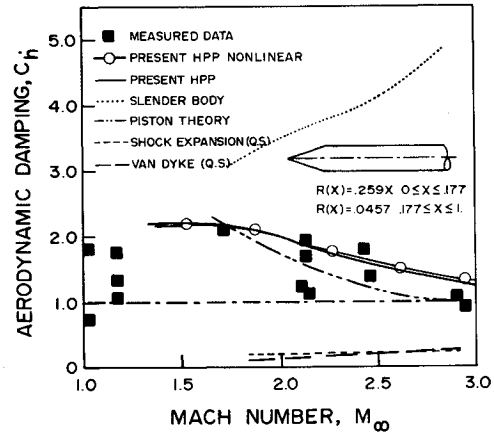

Fig. 11 Aerodynamic damping coefficients vs Mach number for a cone-cylinder vibrating in second-bending mode (data taken from Ref. 14).

be provided by the HPP method, valid in the higher frequency range. Again, good agreement is found between the present results and the measured data. To model this complex configuration, less than 100 panels were used in the prescribed frequency range. Consequently, only 30 s CPU time in an IBM 3081 were needed for all data obtained in Figs. 12 and 13 for a single Mach number. Further details of the computed results related to those in Figs. 11, 12, and 13 can be found in Ref. 17. In passing, we should remark that the present inviscid analysis ignores the based flow and the separated flow altogether for all configurations considered. Our objective here is, in fact, to verify our computed results with Hanson and Doggett's measurement in using their SA-1 Launch Vehicle model. This model may be quite different in its configuration from that of the realistic SA-1 launch vehicle, as pointed out by one of the reviewers. Although no issues on separated flow were mentioned in Ref. 16, this reviewer cautioned that on all of the regular Saturn SA-1 launch vehicles, the unsteady aerodynamics were dominated by separated flow effects.[18-21]

IV. Concluding Remarks

For aeroelastic applications in the complete supersonic Mach number range, the HPP method has been extended to include the influence of the mean-flow nonlinearity. Conclusions can be drawn in regard to three aspects: 1) nonlinear effects, 2) computation efficiency and cost effectiveness, and 3) full-frequency applicability.

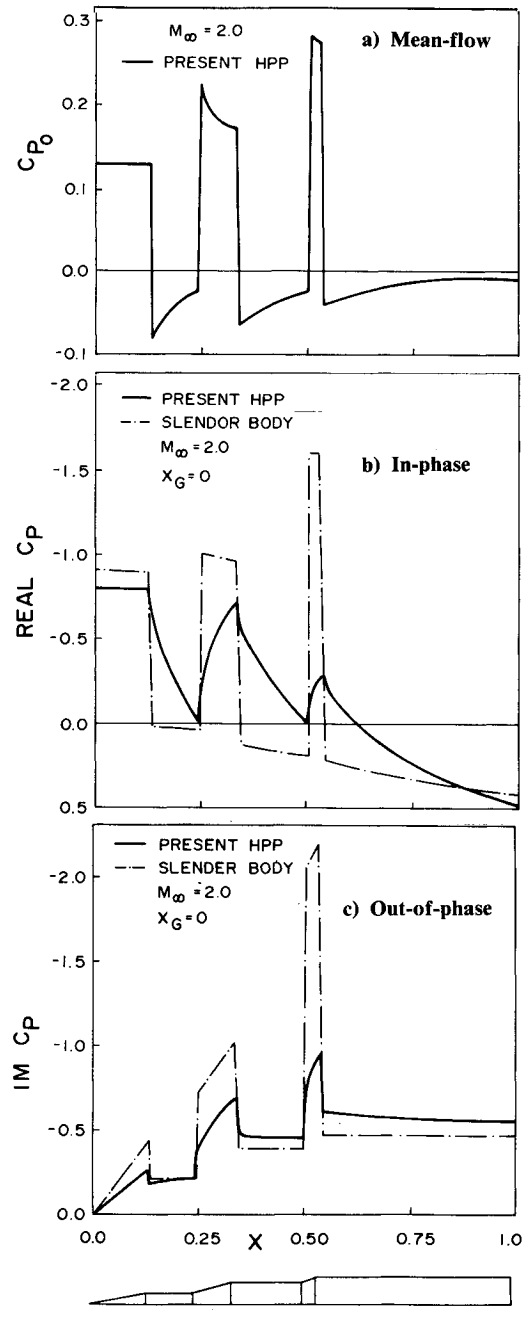

Fig. 12 Pressure coefficients for a Saturn SA-1 configuration at $M_\infty = 2.0$, reduced frequency $k = 1.8$, and center of rotation at the apex.

SATURN SA-I MODEL

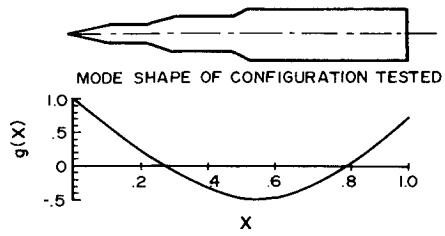

GEOMETRY OF THE CONFIGURATION

R(X)=.2296X	0 ≤ X ≤ .1317
R(X)=.03024	.1317 ≤ X ≤ .241
R(X)=.268X-.03445	.241 ≤ X ≤ .3353
R(X)=.05541	.3353 ≤ X ≤ .5066
R(X)=.4515X-.17332	.5066 ≤ X ≤ .5288
R(X)=.06543	.5288 ≤ X ≤ 1.0

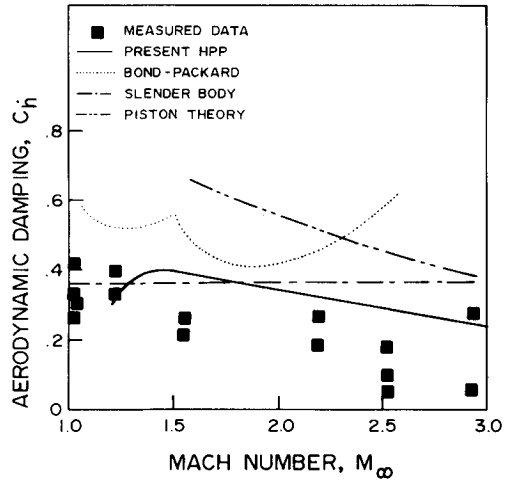

Fig. 13 Comparison of computed and experimental aerodynamic damping coefficients vs Mach number for a Saturn SA-1 configuration vibrating in first-bending mode (data taken from Ref. 16).

First, computed steady pressures and stability derivatives using the HPP nonlinear method compare favorably with the results of other theories. The unsteady HPP-nonlinear results show that the influence of the mean-flow nonlinearity is important. For a slender body, the nonlinear effect becomes more apparent in the high Mach number range. All unsteady nonlinear results correlate better with measured data than those by other methods. Consequently, predicted flutter boundaries are less conservative than those based on the linear or slender-body theories.

Second, the HPP program code is computationally efficient. For example, it requires normally one-tenth of the number of panels used by other surface panel methods. Less than 100 panels are used for a complex configuration such as Hanson and Doggett's Saturn launch vehicle model. Furthermore, the panel number is regulated and is not significantly affected by the Mach number or frequency variations. To compute for each flutter point, a typical case requires no more than three minutes of CPU time in an IBM 3081. The HPP code is, therefore, cost-effective for industrial applications.

Third, to perform flutter analysis for a large space rocket in terms of a scaled model such as Hanson and Doggett's SA-1 launch vehicle, the required range of reduced frequency is by no means small. Thus, accurate predictions can only result from a valid full-frequency code such as the present HPP code.

Once developed, the present method for axisymmetric/asymmetric bodies can be combined with the H-G method for lifting surfaces[2] to yield an engineering tool for aeroelastic applications to wing-body configurations.

Acknowledgment

The present work was supported by the U.S. Army Research Office, Durham, North Carolina; the contract was monitored by Dr. Robert E. Singleton, and Dr. Thomas Doligalski. A part of the computational work, performed by Darrell K. James, is acknowledged.

References

[1]Garcia-Fogeda, P. and Liu, D. D., "A Harmonic Potential Panel Method for Flexible Bodies in Unsteady Supersonic Flow," AIAA Paper 86-0007, 1986.

[2]Chen, P. C. and Liu, D. D., "A Harmonic Gradient Method for Unsteady Supersonic Flow Calculations," *Journal of Aircraft,* Vol. 22, May 1985, pp. 371-379.

[3]Roos, R., Bennekers, B., and Zwaan, R. J., "Calculation of Unsteady Subsonic Flow About Harmonically Oscillating Wing/Body Configurations," *Journal of Aircraft,* Vol. 14, May 1977, pp. 447-454.

[4]Revell, J. D., "Second-Order Theory for Unsteady Supersonic Flow Past Slender, Pointed Bodies of Revolution," *Journal of the Aerospace Sciences,* Vol. 27, Oct. 1960, pp. 730-740.

[5]Van Dyke, M. D., "First and Second Order Theory of Supersonic Flow Past Bodies of Revolution," *Journal of Aeronautical Sciences,* Vol. 18, March 1951, pp. 161-178.

[6]Woodward, F. A., "An Improved Method for the Aerodynamic Analysis of Wing-Body-Tail Configuration in Subsonic and Supersonic Flow," NASA CR-2228, 1973.

[7]Krasnov, N. F., *Aerodynamics of Bodies of Revolution,* American Elsevier Publishing, New York, 1970, pp. 239-263.

[8]Schiff, L. B. and Sturek, W. B., "Numerical Simulation of Steady Supersonic Flow Over an Ogive-Cylinder-Boattail Body," AIAA Paper 80-0066, Jan. 1980.

[9]Brong, E. A., "The Flowfield About a Right Circular Cone in Unsteady Flight," AIAA Paper 65-398, 1965.

[10]Platzer, M. F. and Sherer, A. D., "Dynamic Stability Analysis of Bodies of Revolution in Supersonic Flow," *Journal of Spacecraft and Rockets,* Vol. 5, July 1968, pp. 833-837.

[11]Ashley, H. and Zartarian, G., "Piston Theory: A New Aerodynamic Tool for the Aeroelastician," *Journal of Aeronautical Sciences,* Vol. 23, Dec. 1956, pp. 1109-1118.

[12]Landahl, M. T., *Unsteady Transonic Flow,* Pergamon Press, New York, 1961, p. 19.

[13]Sewell, J. L., Hess, R. W., and Watkins, C. E., "Analytical and Experimental Investigation of Flutter and Divergence of Spring-Mounted Cone Configurations at Supersonic Speeds," NASA TN D-1021, April 1962.

[14]Hanson, P. W. and Doggett, R. V., "Wind-Tunnel Measurements of Aerodynamic Damping Derivatives of a Launch Vehicle Vibrating in Free-Free Bending Modes at Mach Numbers from 0.70 to 2.87 and Comparisons with Theory," NASA TN D-1391, Oct. 1962.

[15]Bond, R. and Packard, B. B., "Unsteady Aerodynamic Forces on a Slender Body of Revolution in Supersonic Flow," NASA TN D-859, May 1961.

[16]Hanson, P. W. and Doggett, R. V., "Aerodynamic Damping of a 0.02-Scale Saturn SA-1 Model Vibrating in the First Free-Free Bending Mode," NASA TN D-1956, Sept. 1963.

[17]James, D. K., Garcia-Fogeda, P., and Liu, D. D., "An Investigation of Aeroelastic Instabilities of the Saturn SA-1 Launch Vehicle Using HPP Method," Arizona State University, Rept. CR-R-86006.

[18]Ericsson, L. E. and Reding, J. P., "Analysis of Flow Separation Effects on the Dynamics of a Large Space Booster," *Journal of Spacecraft and Rockets,* Vol. 2, July-Aug. 1965, pp. 481-490.

[19]Ericsson, L. E., "Aeroelastic Instability Caused by Slender Payloads," *Journal of Spacecraft and Rockets,* Vol. 4, Jan. 1967, pp. 65-73.

[20]Ericsson, L. E. and Reding, J. P., "Reynolds Number Criticality in Dynamic Tests," AIAA Paper 78-166, Jan. 1978.

[21]Ericsson, L. E. and Reding, J. P., "Dynamic Simulation Through Analytic Extrapolation," *Journal of Spacecraft and Rockets,* Vol. 19, March-April 1982, pp. 160-166.